



Myelin repair is fostered by the corticosteroid medrysone specifically acting on astroglial subpopulations

Markley Silva Oliveira Junior,^a Jessica Schira-Heinen,^a Laura Reiche,^a Seulki Han,^a Vanessa Cristina Meira de Amorim,^b Isabel Lewen,^a Joel Gruchot,^a Peter Göttle,^a Rainer Akkermann,^a Kasum Azim,^{a,1} and Patrick Küry^{a,1*}

^aDepartment of Neurology, Neuroregeneration laboratory, Medical Faculty, Heinrich-Heine-University, Düsseldorf 40225, Germany

^bInstitute for Stem Cell Research and Regenerative Medicine, Medical Faculty, Heinrich-Heine-University, Düsseldorf 40225, Germany

Summary

Background Multiple sclerosis is characterised by inflammation, oligodendrocyte loss and axonal demyelination and shows an additional impact on astrocytes, and their polarization. Although a certain degree of spontaneous myelin repair can be observed, disease progression, and aging impair regeneration efforts highlighting the need to better understand glial cell dynamics to establish specific regenerative treatments.

Methods Applying a chronic demyelination model, we here analysed demyelination and remyelination related effects on astrocytes and stem cell niches and studied the consequences of medrysone application on myelin repair, and astrocyte polarization.

Findings Medrysone induced recovery of mature oligodendrocytes, myelin expression and node formation. In addition, C3d/S100a10 co-expression in astrocytes was enhanced. Moreover, Timpr1 expression in C3d positive astrocytes revealed another astrocytic phenotype with a myelination promoting character.

Interpretation Based on these findings, specific astrocyte subpopulations are suggested to act in a myelin regenerative way and manner the regulation of which can be positively modulated by this corticosteroid.

Funding This work was supported by the Jürgen Manchot Stiftung, the Research Commission of the medical faculty of the Heinrich-Heine-University of Düsseldorf, the Christiane and Claudia Hempel Foundation for clinical stem cell research and the James and Elisabeth Cloppenburg, Peek and Cloppenburg Düsseldorf Stiftung.

Copyright © 2022 The Authors. Published by Elsevier B.V. This is an open access article under the CC BY-NC-ND license (<http://creativecommons.org/licenses/by-nc-nd/4.0/>)

Keywords: Reactive astrogliosis; Multiple sclerosis; Corticosteroids; Cuprizone; Remyelination; Subventricular zone

Introduction

Oligodendrocyte loss and sustained myelin damage leading to axonal demyelination are main features of the inflammatory demyelinating disease Multiple sclerosis (MS). As a result, axonal nutrition and signal propagation are impaired eventually leading to irreversible functional deficits. Oligodendroglial precursor cells (OPCs) and neural stem cells (NSCs) can confer a certain degree of oligodendroglial cell replacement and myelin repair, the efficiency of which declines with disease progression and age.¹ Moreover, astrocyte

activation and gliosis are observed additionally modulating endogenous repair processes.^{2,3} This also holds true for nearby neurogenic stem cell niches, such as the subventricular zone (SVZ), with gliosis, and its upgrading inflammation leading to NSCs depletion.^{3–5} As these NSCs contribute to neuronal, oligodendroglial and astroglial cell populations, thereby supporting axon integrity, neuronal communication and myelination this must be considered as a substantial impact.^{6–8} Oligodendroglial cells are preferentially generated within the dorsal region (d-SVZ)^{7–10} whereas astrocytes mainly develop from the lateral SVZ.^{7,11} Nonetheless, under pathological conditions astrocytes can also be generated in the d-SVZ and populate nearby sites.^{12,13} The d-SVZ can be further subdivided in 3 micro-niches: (i) medial-

*Corresponding author.

E-mail address: kuery@uni-duesseldorf.de (P. Küry).

¹ These authors contributed equally.

Research in context

Evidence before this study

At every 5 minutes, someone is diagnosed with Multiple sclerosis worldwide. Affecting young adults through neuroinflammation and demyelination episodes, this disease aggravates over ageing, imposing the patient to severe symptoms such as fatigue, loss of vision, numbness, mobility problems, pain, cognitive, and memory deficits. Drug-repurposing approaches can be of great help to find new treatments, particularly for the still unmet clinical need of fostering endogenous repair activities. By applying a preclinical model of chronic demyelination, we investigated the effects of medrysone, an ophthalmic anti-inflammatory corticosteroid, in the context of oligodendrocyte replacement, and axon remyelination *in vivo*.

Added value of this study

This study focused on the remyelinating potential of medrysone. We validated its activity in cultured primary oligodendroglial precursor cells by assessing pro-myelination gene activities, and myelin protein expression, which were, however, not directly affected by this drug. Nevertheless, TNF- α induced neurotoxic astrocytes treated with medrysone recovered a non-neurotoxic profile. Subsequently, chronically demyelinated mice fed with cuprizone, a copper chelator, were treated with this corticosteroid. Medrysone substantially promoted corpus callosum remyelination, and a number of beneficial features related to different astrocyte subpopulations were regulated by this drug. While therefore highlighting this drug's potential as a novel Multiple sclerosis treatment, this study also clearly demonstrates a functional involvement of astroglial cells in central nervous system repair - the successful pharmacological modulation of which has so far not been reported.

Implications of all the available evidence

Under *in vivo* circumstances, medrysone stimulated remyelination by boosting oligodendrocyte recruitment, axonal myelination, and nodes of Ranvier restoration. Nonetheless, effects were mediated in a non-direct way and an astrocyte heterogeneity signature particularly correlated to a regenerative potential was specifically modulated by medrysone. Our observations strongly support the notion that cellular processes others than those directly affecting oligodendroglia are indeed applicable for the identification of myelin repair promoting drugs. Our study includes a diversity of experimental methods with different cell subtypes identified and observing distinct brain structures evolutionary conserved between humans and mice, strengthening our suggestion of medrysone as a suitable molecule for biomedical translation.

dorsal SVZ (where the medial and dorsal wall are connected), (ii) middle-dorsal SVZ (the centre area of the d-

SVZ), (iii) dorsal-horn SVZ (where the lateral and dorsal wall create a corner; see Figure 1C and 1C') all of which found to display differences in terms of progenitor generation in health and disease.^{9,14–16}

Studies utilizing the demyelinating compound cuprizone (CPZ) have shown that SVZ dependent oligodendrogenesis, hence, myelin restoration/ cell replacement can be more efficient as from parenchymal OPCs,^{2,17} highlighting the SVZ as critical structure for repair. Nevertheless, the involvement of reactive astrocytes in respect of their heterogeneity throughout the d-SVZ and within adjacent areas have not been well described so far. Initial reports relate to oligodendrocyte loss dependent on reactive astrocytes, up-regulating interleukins and complement factors^{18–20} or to promote remyelination and OPCs/NSCs maturation depending on trophic factors released by resident astrocytes.^{21,22} Reactive astrocytes were basically divided into neurotoxic/A1, and neuroprotective/A2 subtypes.²³ Whereas neurotoxic astrocytes regularly express complement factor 3d (C3d),^{24,25} neuroprotective commonly express S100a10, known to be involved in tissue repair.^{26–28} Moreover, transcriptomic evaluations have recently shown that some astroglial cells even express A1 and A2 molecules concomitantly, thereby leading to a “hybrid” phenotype that appears to contribute to brain regeneration,^{29,30} hence, supporting the fact that A1/A2 labelling is outdated to define astrocytic function. More recently, Escartin and colleagues³¹ published a consensus statement defining some key variables to properly characterize reactive astrogliosis such as protein co-expression, time, disease and region analysed (diseased or healed), and our study is based on these variables.

Fostering myelin repair in patients with demyelination diseases is still an unmet clinical need³² and considering the here described cellular heterogeneity and the diverse and complex contributions of different phenotypes to successful tissue repair we investigated the impact of medrysone to white matter regeneration. This FDA-approved anti-inflammatory corticosteroid has recently been identified as potential neuroregenerative compound in the context of NSCs³³ and was applied here to mice suffering to sustained/chronic demyelination of the corpus callosum.

Methods

Ethics statement for animal experiment

Transgenic hGFAP-GFP promoter mice³⁴ [FVB/N-Tg (GFAPGFP) 14mes/J; Jax stock number: Cat#003257, female and male] provided by Prof. Dr. Nikolaj Klöcker (Medicine Faculty, Heinrich-Heine-University, Düsseldorf, Germany) mice were housed in a pathogen-free facility with 12 hours light/dark cycle and supplied with nutrition and hydration *ad libitum*. *In vivo* experiments were performed in adult mice of

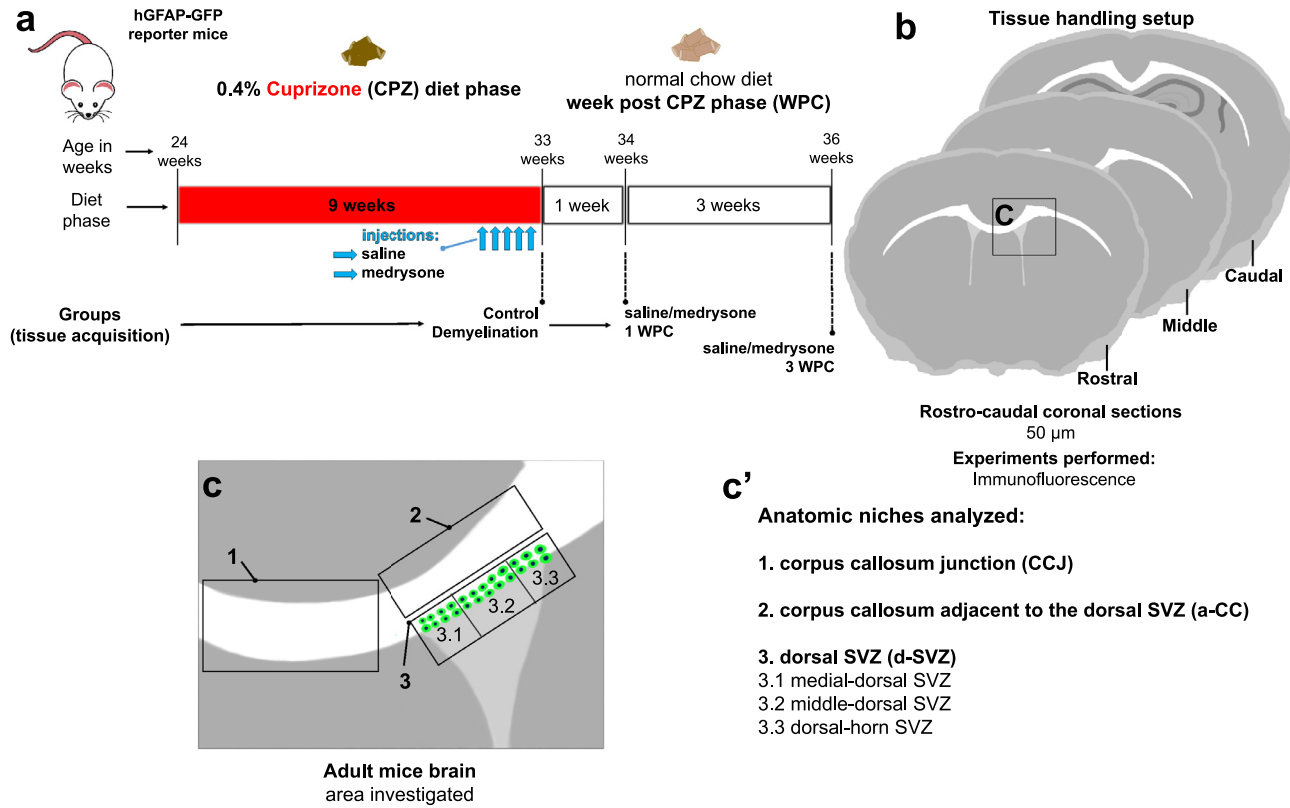


Figure 1. CPZ experimental setup. (a) Timeline of CPZ induced demyelination and of medrysone treatment in adult (24 weeks old) hGFAP-GFP reporter mice. CPZ treatment lasted for 9 weeks, then either medrysone- or saline solutions were applied intraperitoneally (i.p.) starting at five days before the end of the CPZ feeding period. Mice were sacrificed after one or three weeks post-CPZ. For additional controls, healthy mice and CPZ fed mice without treatment were sacrificed. (b) Rostrocaudal directed coronal brain slices were collected between 0.745mm to -1.25mm Bregma, and then analysed using immunofluorescence. (c,c') The corpus callosum junction (CCJ), corpus callosum adjacent to the dorsal-SVZ (a-CC) and dorsal-SVZ (divided in micro-domains: 1-medial dorsal SVZ, 2-middle dorsal SVZ, 3-dorsal horn SVZ) were the anatomic niches investigated.

either sex (from 24 weeks until 36 weeks of age). For primary astrocyte and OPC monocultures 0 or 1 day old neonatal Wistar rats of either sex were utilized. The Review Board for the Care of Animal Subjects of the district Government (LANUV, North-Rhine Westphalia, Germany) approved all research procedures under the following ethic approval numbers: Az.:8102.04.2019.A20 for *in vivo* experiments, O69/11 and V54/09 for *in vitro*. Any other details have been listed in the ARRIVE checklist.

Primary astrocyte monoculture

Primary astrocyte cultures were generated from postnatal rats (Wistar, 0–1 day old) according to McCarthy and de Vellis.³⁵ Brains were collected from the rat's skull and rinsed on MEM-Hepes medium (Life Technologies; Cat#12360038). The hemispheres were separated and cut off, meninges were removed, and the remaining cortices were cut into small pieces. The tissue was collected in centrifuge tubes containing 50 ml MEM-Hepes medium and spun down for 1 minute (min) at 2000 rpm. The tissue pellet was then triturated 10 times with a flame-polished Pasteur pipette and passed through a 40 μm cell strainer. Afterwards, the cell suspension was split onto 2 T-75 flasks and 20 ml of astrocyte medium [DMEM-low glucose (Life Technologies, Cat#D6046), 10% fetal calf serum (FCS; Gibco, Cat#10500-064), 2 ml of L-glutamine (Life Technologies, Cat#G7513), 50 units per ml of penicillin/streptomycin (Life Technologies, Cat#P4333)], each. The medium was changed 3 times a week, and after 10 days, flasks were placed onto a shaker (Excella E24 incubator, 4 h, 180 rpm, 37°C) to remove all microglial and dead cells. Afterwards, remaining astroglia were washed with Dulbecco's phosphate buffer solution (DPBS; Life Technologies, Cat#14190144), and subsequently 5 ml of trypsin was added for 5 min at 37°C and 5% CO₂. The reaction was stopped by adding astrocyte medium and the cell suspension collected into a 50 ml Falcon tube. Cells were centrifuged at 1200 rpm for 5 min, and the supernatant was completely aspirated afterwards. Afterwards, magnetic activated cell sorting (MACS; Miltenyi Biotec, Cat#130707677) was performed according to the manufacturer's protocol to purify the culture. Briefly, the cell pellet was resuspended in 80 μL of PB buffer (0.5% bovine serum albumin, Capricorn, Cat#FBS-16A in DPBS) and 20 μL of anti-Glast (ACSA-1; Miltenyi Biotec, Cat#130095822; RRID:AB_10829302) biotin antibodies were added, well mixed and incubated for 10 min at 2–8°C. 2 ml of cold PB buffer were added and the cells centrifuged at 1200 rpm for 5 min. The supernatant was removed, and cells were resuspended again in 80 μL of the cold PB buffer. 20 μL of anti-biotin microbeads were added, mixed, and incubated for another 15 min at 2–8°C. The cells were washed with 2 ml cold PB buffer and centrifuged at 1200 rpm for

5 min, the supernatant was removed, and cells were resuspended in 500 μL of buffer. For magnetic separation, the columns were placed in the magnetic field within 500 μL buffer per column. The cell suspension was disposed in it, and the columns were washed 3x with 500 μL of buffer; the magnetically labelled cells were flushed out by pressing the plunger within the column. The cell suspension was centrifuged for 5 min at 1200 rpm, and the supernatant was fully removed; the cells were resuspended in astrocyte medium. Purified astrocytes were cultured for 3 days onto 0.25 mg/ml poly-D-lysine coated (PDL, Sigma-Aldrich; N/A) glass coverslips (13 mm) in 24-well plates (for immunocytochemistry; 6.0×10^4 cells/well) or 0.25 mg/ml PDL coated 24-well plates for quantitative reverse transcription-polymerase chain reaction (qRT-PCR; 5×10^4 cells/well). Astrocytes were subjected to 0.1 % Dimethylsulfoxide (DMSO, Sigma Aldrich, Cat#D2650), 30ng/ml tumour necrosis factor-alpha (TNF- α , R&D System, Cat#510RT) or 2.5 μM medrysone (6 α -methyl-11 β -hydroxy-Progesterone; Cayman Chemical, Cat#19533) for 48 hours. Astrocyte monocultures were between 95 and 98% pure as revealed by Gfap/Glast double immunostaining (data not shown). The number of animals per analysis was at least n=10 per experiment for *in vitro*/cell culture experiments, given that primary cells are generally generated from 10 neonatal rats and then pooled. Nevertheless, reproduction and statistical evaluation of such experiments was then undertaken by performing 3–4 different and independent experiments. Sample sizes for our *in vitro*/cell culture experiments are based on our (published) experience with primary neural cell types.

Primary OPC monoculture

Primary OPC cultures were prepared from Po-1 Wistar rats according to McCarthy and de Vellis³⁵ with modifications by our group.^{36–38} Primary OPCs (>97 % pure) were either seeded onto 0.25 mg/ml PDL coated glass coverslips (13 mm) in 24-well plates (for immunocytochemistry; 2.5×10^4 cells/well) or 0.25 mg/ml PDL coated 24-well plates for qRT-PCR (5×10^4 cells/well) in high-glucose DMEM-based Sato medium [(5 $\mu\text{g}/\text{ml}$ bovine insulin; 50 $\mu\text{g}/\text{ml}$ human transferrin; 100 $\mu\text{g}/\text{ml}$ bovine serum albumin fraction V (BSA; Thermo Fisher Scientific); 6.2 ng/ml progesterone; 16 $\mu\text{g}/\text{ml}$ putrescine, 5 ng/ml, sodium selenite; 400 ng/ml T3 (tri-iodo-thyronine); 400 ng/ml T4 (thyroxin; all Sigma–Aldrich unless stated otherwise); 4 mM L-glutamine; 100 U/ml penicillin/0.1 mg/l streptomycin (both Thermo Fisher Scientific)]. After 1.5 hours, cell differentiation was induced by changing to differentiation medium (Sato medium supplemented with 0.5 % FBS). The medium was exchanged every 3 days. OPCs were supplemented with 0.1 % DMSO or 5 μM medrysone for 72 hours without medium exchange. Primary OPC

cultures were on average 95% pure based on Gfap, Iba-1 staining for contaminating astrocytes and microglia, respectively (data not shown). The number of animals per analysis was at least $n=10$ per experiment for in vitro/cell culture experiments, given that primary cells are generally generated from 10 neonatal rats and then pooled. Nevertheless, reproduction and statistical evaluation of such experiments was then undertaken by performing 3-4 different and independent experiments. Sample sizes for our in vitro/cell culture experiments are based on our (published) experience with primary neural cell types.

Immunocytochemistry

Astrocytes were incubated with 0.5 % Triton X-100 (Sigma Aldrich) in DPBS for 30 minutes (min), followed by a 60 min incubation with blocking solution containing 10 % normal goat serum (NGS, Gibco, Cat#PCN5000) in DPBS supplemented with 0.5 % Triton X-100 (Sigma Aldrich, Cat#85111) and 10 % BSA. Primary antibodies for astrocytes were diluted in blocking buffer with following concentrations: Chicken anti-gial fibrillary acid protein (Gfap; 1:500, Aves labs, Cat#SKU:Gfap; RRID: AB_2307313); Rabbit anti-complement component 3d (C3d; 1:300, Dako, Cat#A0063; RRID: AB_578478). OPCs were blocked with 10% NGS in DPBS containing 0.1% Triton X-100 at RT for 45 min. Primary antibodies for OPCs were diluted in 10% NGS in DPBS containing 0.01% Triton X-100 with following concentrations: Rat anti-myelin basic protein (MBP; 1:250, Biorad, Cat#aa8287, RRID:AB_32500). Primary antibody incubations were performed overnight. Secondary antibodies were all used at 1:500 [anti-rabbit AlexaFluor 594 (Cat#A32740; RRID: AB_2762824); anti-chicken AlexaFluor 488 (Cat#A32931; RID:AB_2762843); anti-rat AlexaFluor 488 (Cat#A-11006; RRID:AB_2534074)]; all from Thermo Fisher Scientific). 4',6'-diamino-2-phenylindole (Dapi, Roche diagnostic GmbH) was applied at a concentration of 5 μ M nuclear dye. Secondary antibodies and dye incubation were performed for 120 min. Coverslips were mounted with Immu-mount (Thermo Fisher Scientific, Cat#1900331) on a glass-slide for subsequently confocal microscopy.

RNA preparation, cDNA synthesis and quantitative RT-PCR analysis

Total RNA purification from OPC and astrocyte monocultures was done using 350 μ L of RLT lysis buffer (Qiagen, Cat#1015762) supplemented with β -mercaptoethanol (1:100, Sigma, Cat#M3148-25). The total RNA was purified by utilizing RNeasy Mini Kit according to manufacturer instructions including DNase digestion. Before quantitative real-time polymerase chain reaction (qPCR), reverse transcription with 250 ng RNA measured using a

NanoDropND 1000 was done using the High-Capacity cDNA Reverse Transcription Kit (Thermo Fisher Scientific, Cat# N8080234). Gene expression levels were determined on a 7900HT sequence detection system (Applied Biosystems, Thermo Fisher Scientific), applying Sybr-Green universal master mix (Thermo Fisher Scientific, Cat#4367659). Following amplification primers were used: For OPCs rat (rt) Gapdh: fwd- GAA CGG GAA GCT CAC TGG C, rev- GCA TGT CAG ATC CAC AAC GG (as reference gene); rtMyrf: fwd- CCT GTG TCC GTG GTA CTG TG, rev- TCA CAC AGG CGG TAG AAG TG; rtPdgfra: fwd- AGC TCT CTG TTC CCA ATG CC, rev- GCC TCC ATT CTG GAG CTT GT; rtSox10: fwd- GTC AGA TGG GAA CCC AGA GCA C, rev- CCC GTA GCC AGC TGC CGA G; rtCNpase: fwd- GCC GTT GTG GTA CTT CTC CA, rev- GCC CGA AAA AGC CAC ACA TT. For astrocytes rtHprt: fwd- CAG TCC CAG CGT CGT GAT TA, rev- ATG GCC TCC CAT CTC CTT CA (as reference gene); rtGfap: fwd- CTG GTG TGG AGT GCC TTC GT, rev- CAC CAA CCA GCT TCC GAG AG; rtSerpina3n: fwd-GGG CAG GTG CTT CGT, rev-AGC GCC TTT GTC TTT CTT TCT G; rtLcn2: fwd-TCT CAG GCC CAC CAT GAT AGA, rev-CAG GTT GTA GTC AGC AGA GAT GGA; rtSerpinger: fwd-GAC AGC CTG CCC TCT GAC A, rev-GCA CTC AAG TAG ACG GCA TTG; rtC3: fwd- CCT TCC CGG GAG CAT CA, rev- GGG CAT ACC CAG CAA TGG; rtC1qa: fwd- CAG AAC CCA CCG ACG TAT GG, rev- TCC TGG TTG GTG AGG ACC TT; rtIL6: fwd- GTT GTG CAA TGG CAA TTC TGA, rev-TCT GAC AGT GCA TCA TCG CTG; rtPt3: fwd- GGC CAA AAG TCA CCC TGT TC, rev- CCA TTC TTT TCT TGG CCA ATCT; rtCd14: fwd- ACA ACA GGC TGG ATA GGA AAC C, rev-TGA CAG GCT CCC CAC TTC AG; rtS100a10: fwd-GCC ATC CCA AAT GGA GCA T, rev- CCC CTG CAA ACC TGT GAA AT

(all primers manufactured by Eurofins genomics, Germany).

Cuprizone diet and drug-treatment procedure

To induce demyelination, 24 weeks old hGFAP-GFP reporter mice were exposed to a regular diet of 0.4 % CPZ (Sniff, Cat#V1534) for nine weeks. Animals were randomized into treatment arms, whilst making sure that the sex matched between groups. Our analyses were based on two arm-randomizations and two-tailed statistical tests to assess how medrysone affected spontaneous remyelination. During the last five days of CPZ feeding, mice received daily intraperitoneal injections of 500 μ L of 0.5 % saline solution or of 5 mg/kg b.w. medrysone [first diluted in DMSO (20 mg/ml stock solution), thereafter diluted using saline to a 7.25 % final concentration of DMSO]. For recovery, mice received normal food for one or three weeks after CPZ feeding (see Figure 1A). Six groups were analysed: (i) control/non-CPZ fed; (ii) 9 weeks CPZ /demyelination; (iii-iv) 9 weeks CPZ, plus saline injection and one or

three weeks of normal food (saline 1/3 WPC respectively); (v-vi) 9 weeks CPZ, plus medrysone injection and one or three weeks of normal food (medrysone 1/3 WPC respectively). We measured the body weight of the animals since CPZ is known to have an impact on body weight. Immunohistochemical analysis was performed on rostrocaudal brain sections (bregma: 0.745 μ m to -1.25 μ m) analysing the corpus callosum junction (Figure 1C' area 1), adjacent corpus callosum (a-CC; Figure 1C' area 2) and the d-SVZ (Figure 1C' area 3; divided into three micro-domains: 3.1-medial dorsal-SVZ; 3.2-middle d-SVZ and 3.3-dorsal-horn SVZ). For *in vivo* investigations we used at least n=4 animals per experimental group. Experiments were previously determined using a G*power analysis. This analysis was also necessary to have animal experiments legally granted by the authorities (The Review Board for the Care of Animal Subjects of the district Government (LANUV, North-Rhine Westphalia, Germany).

Tissue processing and immunohistochemistry

For immunohistochemistry mice were transcardially perfused with 20 ml ice-cold DPBS and 20 ml 4 % PFA and dissected brains were post fixed with 4 % PFA 48 hours. Subsequently, brains were incubated with 30 % sucrose for 72 hours, embedded in 2 % agarose and cut into 50 μ m thick sections using a vibration microtome. Sections were permeabilised by incubation with 0.5 % Triton X-100 for 30 min, blocked with 10 % NGS supplemented with 5 % BSA and 1% Triton for 120 min and incubated with following antibodies overnight at 4 °C: rat anti-MBP (rat; 1:300, Biorad, Cat#aa8287, RRID: AB_32500); mouse anti-adenomatous polyposis coli (CCr-APC; 1:300, anti-APC-Ab7-clone CCr, Merck millipore, Cat#OP80, RRID: AB_2057371); rabbit anti-glutathione S-transferase-pi (GST π ; 1:500, Enzo, Cat#ADIMSA101, RRID: AB_10615079); rabbit anti-oligodendrocyte transcription factor 2 (Olig2; 1:500, Millipore, Cat#AB9610, RRID:AB_570666); mouse anti-contactin associated protein 1 (Caspr; 1:400, anti-Caspr-paranodin, neuroxin-IV, clone k65/35, Neuromab, Cat#75-001, RRID: AB_10671175); rabbit anti-sex-determining region Y-box 1- (Sox10; 1:100, DCS immunoline, Cat#S1058C002, RRID: AB_2313583); mouse anti-breast carcinoma-amplified sequence 1 (Bcas1/NaBC1; 1:200, Santa Cruz, Cat#sc-136342, RRID: AB_10839529); chicken anti-green fluorescent protein (GFP; 1:500, Aves labs, Cat#GFP1010, RRID: AB_2307313); rabbit anti-human C3d (1:500, Dako, Cat#A0063; RRID: AB_578478); mouse anti-signal transducer and activator of transcription 3 (Stat3; 1:400, Invitrogen, Cat#MA1-13042, RRID: AB_10985240); mouse anti-human S100 calcium-binding protein A10 (S100a10; 1:500, Thermo Fisher Scientific, Cat#MA5-15326, RRID: AB_2092361); rabbit anti-myelin proteolipid protein (PLP; 1:250, kind gift from Dr. B. Trapp,

Department of Neurosciences, Cleveland Clinic, Ohio, United States; Chen et al., 2015); goat anti-tissue metalloproteinase inhibitor 1 (Timp1; 1:100, R&D System, Cat#AF580, RRID:AB_355455); goat anti-lipocalin-2/NGAL (Lcn2; 1:180, R&D System, Cat#AF1857, RRID: AB_355022); rabbit anti-nitric oxide synthase (iNOS; Abcam, Cat#ab95441, RRID:AB_10688716); rat anti-nuclear factor-erythroid factor 2-related factor 2 (Nrf2; 1:100, Cell Signalling Technology, Cat#14596, RRID: AB_2798531); rabbit anti-transcription factor Mafg (Mafg; 1:100, Genetex, Cat#GTX114541, RRID: AB_10619599); mouse anti-epidermal growth factor receptor (Egfr; 1:500, Anti-Egfr endoplasmic domain, Millipore, Cat#8662051047, RRID: AB_2096607). Antigen retrieval disrupts the GFP signal, thus, it was used only for anti-MBP, anti-Olig2 (Figure 1), anti-Sox10 (Figures 1 and 6) and anti-PLP (Figure 6) staining. For this purpose, sections were rinsed in 0.1 M phosphate buffer (pH 7.4) for 3 \times 5 min, transferred to 10 mM sodium citrate buffer (pH 8.5) pre-heated to 80 °C in a water bath for 20 min and rinsed 0.1 M phosphate buffer (pH 7.4) for 3 \times 5 min before blocking and incubation with primary antibodies. After incubation with primary antibodies, sections were washed and incubated with secondary antibodies and Dapi for 120 min. All secondary antibodies were used at a concentration of 1:200 [anti-rat AlexaFluor 647 (Cat#A-11006; RRID: AB_2534074); anti-mouse AlexaFluor 594 (Cat#A32742; RRID:AB_2762825); anti-rabbit AlexaFluor 647 (Cat#A32733; RRID:AB_2633282); anti-chicken AlexaFluor 488 (Cat#A32931; RID:AB_2762843); anti-mouse AlexaFluor 647 (Cat#A32728; RRID:AB_2633277), Donkey anti-goat AlexaFluor 594 (Cat#A32758; RRID: AB_2762828), all Thermo Fisher Scientific]. Subsequently, sections were washed in DPBS and mounted onto glass slides (Superfrost Ultra Plus, Thermo Fisher Scientific).

All sections were analysed using a confocal laser scanning microscope (CLSM) 510 (Zeiss, 510, Carl Zeiss AG, Oberkochen, Germany). Rostral, middle and coronal sections each 50 μ m thick were utilized for cell quantification for each individual, totalizing an area of observation of 150 μ m in a z-stack orientation. For quantification, areas corresponding to 150 μ m of the junction corpus callosum and to 100 μ m of the d-SVZ were analysed per section. Z-stack orientation was performed and at least 35 slices per Z-stack file were taken for each sample. For MBP and PLP fluorescence at the CCJ and a-CC respectively (see Figure 1C') photomicrographs were analysed using the software Fiji-ImageJ version 1.47³⁹ using a virtual line traced around the region of interest (ROI) to determine fluorescence units. No normalization of ROIs was performed within the histogram algorithm. By using the ImageJ software, a square of 280 μ m \times 220 μ m (standardised by using the ImageJ dimension rule) was drawn on each picture obtained for MBP and PLP quantification. Moreover, by using the histogram algorithm the

fluorescence intensity was quantified within the squared area – being aware that the corpus callosum at both CCJ and a-CC areas changes in thickness and size and that our evaluation was based on rostral, middle and caudal orientation.

Statistical analysis

Data are shown as mean values \pm standard error of the mean (mean \pm SEM). GraphPad Prism 7.0.2 (GraphPad Prism, San Diego, CA, RRID: rid_000081) was used for statistics and graphics collection. To assess the absence of Gaussian distribution, Shapiro–Wilk normality test was used for all datasets. Student's t-test was applied for comparing two groups and two-way analysis of variance (ANOVA) with Bonferroni post-test for multiple comparisons was applied to compare three or more groups. For data sets not passing the Shapiro–Wilk normality test, Kruskal–Wallis test with Dunn's post-test for multiple comparisons of three or more groups was applied. P values are defined as follows: * represents $p \leq 0.05$; ** represents $p \leq 0.01$; *** represents $p \leq 0.001$. Asterisks absence means no statistically significant difference was observed. Absent bars in certain groups indicate that the respective cell subtype was not found, these groups were not considered for the statistical analysis. A priori sample size calculation for the *in vivo* experiments was performed using the G*Power 3.1.9.2 software⁴⁰ (test family: t-tests; statistical test: means: Wilcoxon-Mann-Whitney test (two groups); tails: two; effect size d: 2.6; alpha error 0.05, power 0.95; allocation ratio N₂/N₁: 1; resulting max sample size: 6). This analysis was also necessary to have animal experiments legally granted by the authorities (The Review Board for the Care of Animal Subjects of the district Government (LANUV, North-Rhine Westphalia, Germany). The number of animals per analysis was at least $n=10$ per experiment for *in vitro*/cell culture analyses, given that primary cells are generally generated from 10 neonatal rats and then pooled. Nevertheless, reproduction and statistical evaluation of such experiments was then undertaken by performing 3-4 different and independent experiments. Sample sizes for our *in vitro*/cell culture experiments are based on our (published) experience with primary neural cell types.

Role of funders

The funding source had no role in study design, collection, analysis and interpretation of data or in manuscript writing

Results

In vivo demyelination and drug-treatment procedure

To induce demyelination, 24-week-old transgenic hGFAP-GFP reporter mice were exposed to 0.4 % CPZ for nine

weeks. During the last five days of CPZ feeding, mice received daily intraperitoneal injections of 5 mg/kg of medrysone- or saline solution. Over the post cuprizone phase (WPC), mice received normal food for one or three weeks (Figure 1a). Six groups were analysed: (i) non-CPZ fed/control; (ii) 9 weeks CPZ diet/demyelination; (iii) 9 weeks CPZ, plus saline injection and one week of normal food (saline 1 WPC); (iv) 9 weeks CPZ, plus saline injection and three weeks of normal food (saline 3 WPC); (v) 9 weeks CPZ, plus medrysone injection and one week of normal food (medrysone 1 WPC); (vi) 9 weeks CPZ, plus medrysone injection and three weeks of normal food (medrysone 3 WPC). Immunofluorescence analysis was performed using 50 μ m rostrocaudal coronal sections (1 rostral section, 1 middle section and 1 caudal section per *n*; Figure 1b) analysing the corpus callosum junction (CCJ; Figure 1c' area 1), the corpus callosum adjacent to d-SVZ (a-CC; Figure 1c' area 2) and the d-SVZ (Figure 1c' area 3; divided into three micro-domains: 3.1-medial dorsal-SVZ; 3.2-middle d-SVZ and 3.3-dorsal-horn SVZ). For cell counting 150 μ m were analysed along the z-axis for all anatomic niches (Figure 1c'). For the CCJ an area of interest of 150 μ m along the x/y-axis and, for d-SVZ an area of interest of 100 μ m along the x/y-axis were analysed in terms of cell counts.

Remyelination and nodes of Ranvier recovery are improved by medrysone

We aimed at evaluating the potency of medrysone to improve remyelination in chronically demyelinated mice induced by a prolonged CPZ application. Looking at the CCJ (see Figure 1c) we found after 9 weeks of CPZ diet a diminished MBP expression (Figure 2s) as well as lower numbers of early-stage mature (GST π positive) oligodendrocytes (OL), mature (Olig2/CC1 double-positive) OL and of active myelinating OL (Sox10/Bcas1 double-positive cells; Figure 2t,2u,2v; see Figure 2x for OL maturation stages and representative markers). Adjacent localization of MBP and Caspr was used to identify nodes of Ranvier by their juxtaposition (Figure 2x'). Of note, the number of which was found to be reduced in response to demyelination (Figure 2w) confirming myelin loss. On the contrary, quantitative analysis revealed that medrysone significantly promoted the recovery of MBP expression (Figure 2s), of early-stage mature OL (Figure 2t), of mature OL (Figure 2u) and of active myelinating OL numbers (Figure 2v), as well as of nodes of Ranvier numbers (Figure 2w) reaching levels similar to healthy controls at 1 and 3 weeks post CPZ, respectively.

Demyelination affects hGFAP-GFP cells at the corpus callosum and the d-SVZ

Throughout myelin damage and depending on the inflammatory stage astrocytes exert either detrimental

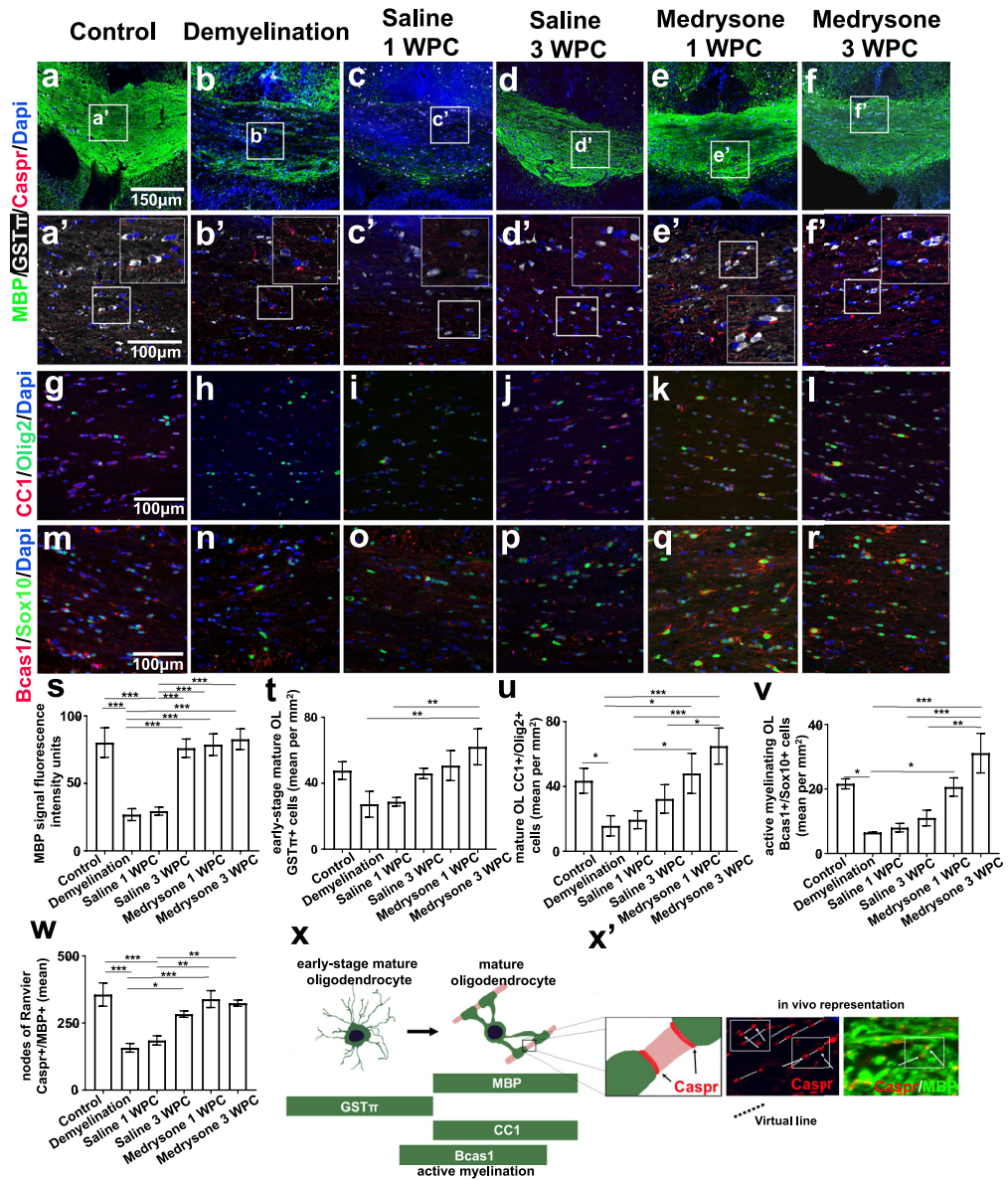


Figure 2. Medrysone promotes oligodendrocyte recovery and remyelination at the corpus callosum junction. Representative pictures of the corpus callosum junction (CCJ, Figure 1c) stained for MBP, GST π , Caspr (a-d, a'-d') Olig2 and CC1 (g-l), Sox10 and Bcas1 (m-r) protein expression. (s) Quantitative analysis of MBP stained structures revealed a decrease of myelin expression in the demyelination group with saline treatment leading to weak remyelination and medrysone significantly promoting MBP recovery at the early time point (1 WPC). (t, u, v) Similarly, the numbers of GST π positive, Olig2/CC1- and Sox10/Bcas1 double-positive cells recovered upon medrysone application accompanied by improved generation of nodes of Ranvier (w). (x) Oligodendrocyte maturation and representative markers (x') graphical and *in vivo* representation of nodes of Ranvier immunofluorescence (Caspr+/MBP+). Bars in (s) correspond to mean fluorescence intensity \pm standard error of the mean (SEM), bars (t, u, v) correspond to mean cell numbers per mm 2 \pm standard error of the mean (SEM), bars (w) correspond to mean number of nodes \pm standard error of the mean (SEM). Statistical significance was calculated using a two-way ANOVA with multiple comparison Bonferroni post-test (* p < 0.05, ** p < 0.01, and *** p < 0.001). Number of animals per analysis: $n=6$ (s, t); $n=5$ (u, v, w). Exact p -values according to sequence from left to right: s: ($p=0.000000383874685$, $p=0.0000009335915998$, $p=0.000001608060795$, $p=0.000000637203217$, $p=0.000000164768189$, $p=0.000004042884687$, $p=0.000001570954253$, $p=0.000000394110251$). t: ($p=0.001937648865078$, $p=0.003177866419346$). u: ($p=0.045380409230564$, $p=0.012638408327068$, $p=0.00011622977178$, $p=0.036252296508041$, $p=0.000318271010733$, $p=0.0117113553263055$). v: ($p=0.023166172011608$, $p=0.04065251019751$, $p=0.000116654567343$, $p=0.000261656183587$, $p=0.001371706447911$). w: ($p=0.000125063209522$, $p=0.000773952216255$, $p=0.018530905333733$, $p=0.000384534736556$, $p=0.001076299627656$, $p=0.002472602001283$, $p=0.007086659102636$).

or beneficial effects which determines or influences remyelination efficacies.^{41,42} After CPZ-mediated chronic demyelination, we found that the degree of GFP-positive cells at the CCJ did not change significantly between groups/pathophysiological stages (Figure 3g). However, when looking at the a-CC, a higher number of GFP-positive cells versus all groups was found in the demyelination, followed by still elevated levels in the medrysone 3 WPC group (Figure 3n), however, without difference to the control. Interestingly, in the d-SVZ, medrysone treated animals at 1 WPC displayed significantly elevated number of transgenic cells which sharply dropped below control levels at 3 WPC (Figure 3o).

Medrysone fosters Stat3 and S100a10 expression in C3d+ astrocytes in the remyelinated CCJ

Depending on the phenotype, astroglial cells can promote demyelination or remyelination.^{25,43,44} Quantification of transgenic cells expressing C3d and signal transducer and activator of transcription 3 (Stat3), revealed that medrysone treatment leads to an increase of C3d+/Stat3+/GFP+ astroglial subpopulation at the CCJ (Figure 4n) and more exclusively at dorsal horn SVZ (Figure S3h). In contrast, demyelination led to an increased number of C3d expressing cells devoid of Stat3 (C3d+/Stat3-/GFP+) which were subsequently reduced or fully depleted in the recovery phase after both saline and medrysone treatment, respectively (Figure 4m). Senescence naturally induces astrocytes to express S100a10.⁴⁵ Nonetheless, during disease, S100a10 expression identifies astrocytes within remyelinated lesions in MS²⁶ as well as upon experimental demyelination.⁴⁷ We performed triple staining for C3d, S100a10 and GFP aiming at identifying reactive astrocytes at the CCJ (Figure 4g-4l). C3d+/S100a10-/GFP+ cells were significantly induced by demyelination (Figure 4o, 4h, 4h') with medrysone counteracting this effect leading to decreased numbers of C3d+/S100a10-/GFP+ cells at both investigated time points (Figure 4o). Our findings revealed that C3d+/S100a10+/GFP+ astrocytes (Figure 4p) appear after demyelination and saline or medrysone treatment but were not detectable in healthy control tissue. Medrysone treatment significantly promoted the C3d+/S100a10+/GFP+ phenotype at 1 WPC which further increased at 3 WPC. Furthermore, C3d-/S100a10+/GFP+ were identified at the CCJ of healthy controls which decreased by demyelination and were not found in saline treated 1 WPC mice, however, it re-appeared at 3 WPC independent of whether animals were saline or medrysone treated (data not shown).

C3d+/Stat3+ and C3d+/S100a10+ astrocytes were regulated at the a-CC throughout remyelination

As a next step, quantification of C3d/Stat3 double-positive, C3d+/S100a10+/GFP+ and C3d-/S100a10+/GFP+

astrocytes in the a-CC (see Figure 1c, 1c') was conducted. C3d+/Stat3-/GFP+ cell numbers were only induced during demyelination then decreasing at saline 1 WPC and being absent in all other groups (Figure 5m; red bars). C3d+/Stat3+/GFP+ cells were not present in control and demyelinated mice (Figure 5a, 5b, 5m), were moderately induced in saline treated animals (Figure 5c, 5d, 5m) and strongly induced upon medrysone treatment at both time points (Figure 5e, 5f, 5m; purple bars). C3d+/S100a10-/GFP+ astrocytes were strongly upregulated upon demyelination and at both remyelination time-points in saline treated mice (Figure 5h, 5i, 5j, 5n; green bars). However, a robust reduction of this phenotype was observed in medrysone treated mice (Figure 5n). C3d+/S100a10+/GFP+ astrocytes rarely appeared over demyelination (blue bars; Figure 5h, 5n). Saline treated mice only showed low levels of this phenotype, whereas medrysone treatment led to a strong increase of C3d+/S100a10+/GFP+ astrocytes at the a-CC at both time points (Figure 5k, 5l, 5n; blue bars).

Demyelination at a-CC was accompanied by DRA or RRA throughout the recovery phase

Chronic demyelination can also decrease levels of myelin proteolipid protein (PLP) and of active myelinating OLs (Sox10+/Bcas1+) in the a-CC, with a weak recovery over saline-treatment (Figure 6e, 6j) and an enhanced recovery upon medrysone treatment (Figure 6d, 6e, 6i, 6j). Lipocalin 2 (Lcn2) it is known for its detrimental activities upon myelin disruption⁴⁶ which acts by controlling inducible nitric oxide synthase (iNOS) expression in glial cells.⁴⁸⁻⁵⁰ We found astrocytes co-expressing Lcn2 and iNOS, identified as demyelination related astrocytes (DRA), which were only found at the a-CC (Figure 1c'). DRA (Lcn2+/iNOS+/GFP+) numbers were significantly increased upon demyelination (Figure 6l, 6m, 6o) with medrysone neutralizing this effect leading to a decreased DRA numbers at both investigated time points (Figure 6n, 6o). Timpr1 is a metallopeptidase inhibitor that has been reported as one of the critical factors released by astrocytes able to promote white matter recovery after demyelination.⁵¹⁻⁵³ We therefore investigated whether reactive astrocytes expressed Timpr1 during recovery phases. By means of Timpr1/C3d/GFP triple staining we identified C3d-negative control astrocytes expressing Timpr1 in healthy tissue. These astrocytes were exclusively found in the a-CC whereas no Timpr1 positive cells were observed at d-SVZ and its micro-domains as well as the CCJ. Moreover, this phenotype was completely absent upon demyelination, during remyelination and in presence of medrysone (data not shown). C3d+ reactive astrocytes expressing Timpr1, however, were absent in healthy and demyelinated tissues, appeared in saline treated animals at both recovery phases and were found to be increased in numbers in

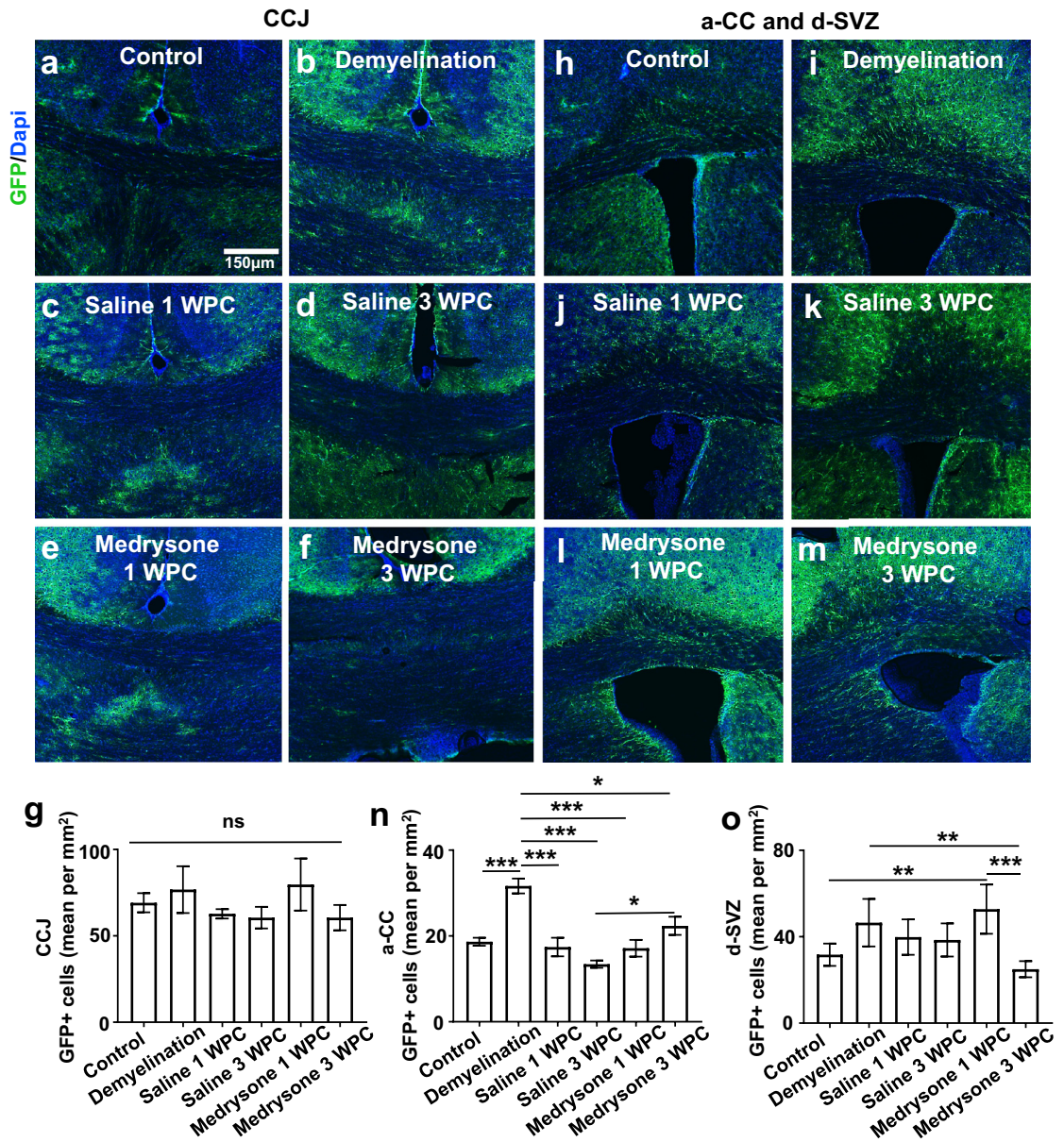


Figure 3. Quantification of hGFAP-GFP positive cells in the corpus callosum junction and dorsal SVZ. (a-m) Representative pictures of GFP-positive cells at the CCJ, a-CC and the d-SVZ with cell nuclei visualized using Dapi. (g) Quantification of GFP-positive cells revealed similar number of GFP expressing cells in all groups at the corpus callosum junction. (n) In the a-CC demyelination induced the degree of GFP-positive cells (versus control) and a mild induction between medryson and saline groups was found at 3 WPC. Moreover, in the d-SVZ (o), GFP-positive cells were enriched upon medryson treatment at 1 WPC (versus control), sharply dropping thereafter (3 WPC). Abbreviation: non-significant (ns). Bars correspond to mean cell numbers per mm² ± standard error of the mean (SEM). Statistical significance was calculated using Kruskal-Wallis test with Dunn's post-test (g) and two-way ANOVA with multiple comparisons Bonferroni post-test (n; o; **p* < 0.05, ***p* < 0.01, and ****p* < 0.001). Number of animals *n*=6 (g, o), *n*=7 (n). Exact *p*-values according to sequence from left to right: n: (*p*=0.000388398742168; *p*=0.000104914644292, *p*=0.000001511008705, *p*=0.000077138716235, *p*=0.019669035728742, *p*=0.028226088991489). o: (*p*=0.006937732126289, *p*=0.005565374980289, *p*=0.000255068999518).

medryson treated mice (Figure 6s, 6t). As this phenotype was exclusively observed over the recovery phase these cells were hence designated as remyelination related astrocytes (RRA). Of note, none of the

C3d/Timp-1 double-positive cells expressed S100a0 (data not shown), indicating that C3d+/S100a0 +/GFP+ astrocytes were probably not participating at this trophic process.

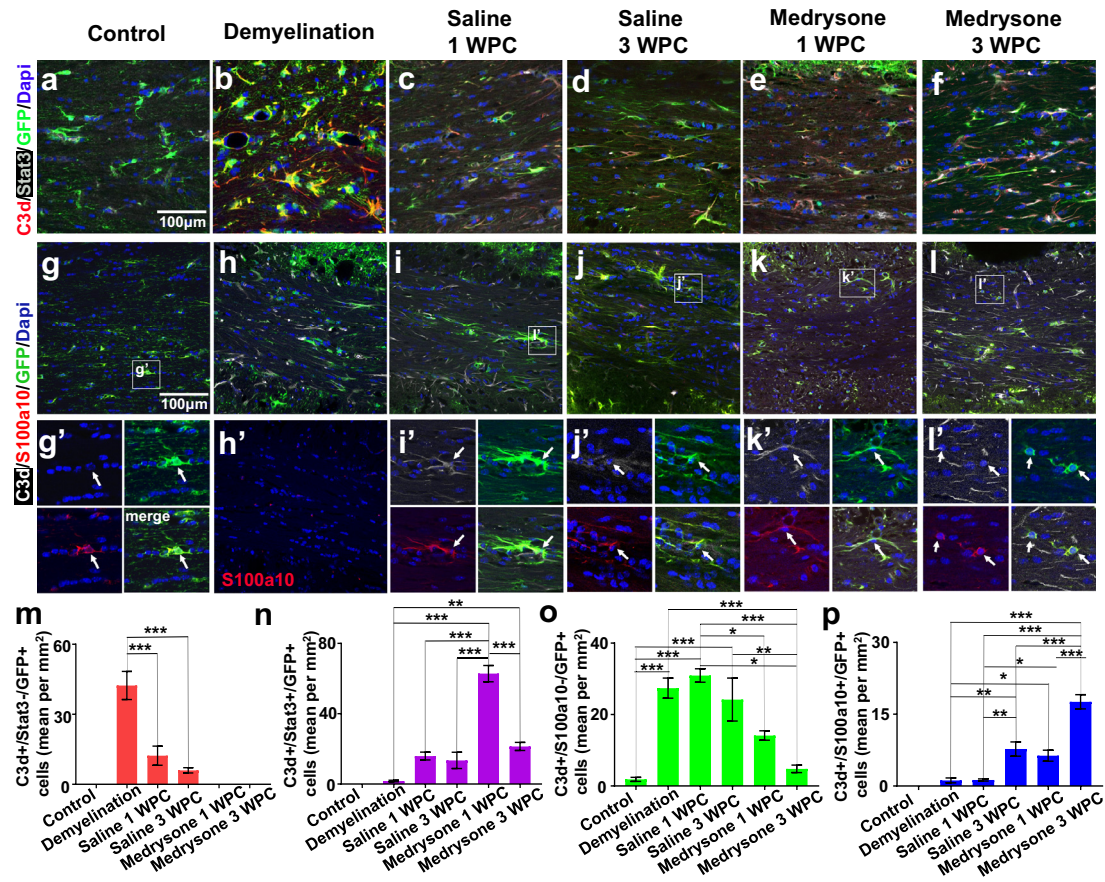


Figure 4. Dynamics of different astroglial subpopulations in the de- and remyelinating corpus callosum. (a-f) Representative pictures of the corpus callosum co-stained for C3d, Stat3 and GFP. (g-l, g'-l') Representative pictures of the corpus callosum co-stained for C3d, S100a10 and GFP. (m) Demyelination enhanced the number of C3d+/Stat3+ astrocytes whereas in the recovery phase they were less present. Medrysone treated mice did not exhibit this astroglial phenotype. (n) Medrysone led to a transient increase of C3d+/Stat3+ astrocytes. (o) C3d+/S100a10+ astrocytes increased after demyelination independent of the treatment, medrysone more effectively reduced this phenotype in both WPC phases. (p) Quantification of C3d+/S100a10+/GFP+ astrocytes revealed that medrysone promoted this phenotype. White arrows point to nuclei of representative cells (g'-l'). Abbreviations: Lateral ventricle (LV). Bars correspond to mean cell numbers per mm² ± standard error of the mean (SEM). Statistical significance was calculated using a two-way ANOVA with multiple comparisons Bonferroni post-test (**p* < 0.05, ***p* < 0.01, and ****p* < 0.001). Number of animals *n*=5 (m-p). Exact *p*-values according to sequence from left to right: m: (*p*=0.000001939212634, *p*=0.000000093452992. n: (*p*=0.0000000001506, *p*=0.003533302378445, *p*=0.000000016322104, 0.000000006736671, 0.000000131339942). o: (*p*=0.0001544193673, *p*=0.000026908283521, *p*=0.000802775438411, *p*=0.000704424040409, *p*=0.015340507431056, *p*=0.000115145119193, *p*=0.003821079590641). p: (*p*=0.004044723153267, *p*=0.036174045580504, *p*=0.000000008760832, *p*=0.004716687589661, *p*=0.042115928088711, *p*=0.000000009715655, *p*=0.000027932768139, *p*=0.000004064840604).

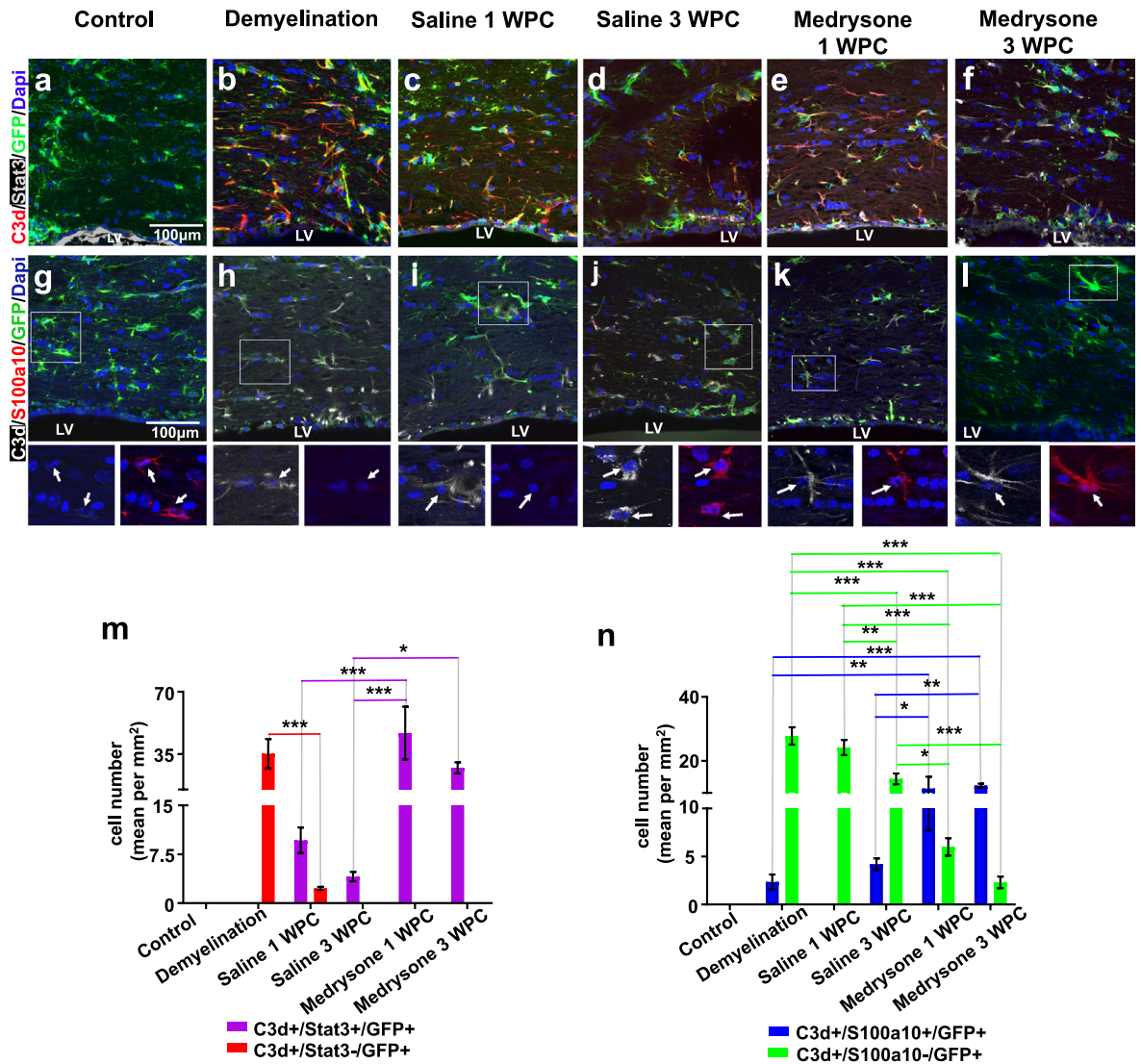


Figure 5. Numbers of C3d+/S100a10+ and C3d+/S100a10- astrocytes change in the adjacent corpus callosum over time and after medrysone treatment. Representative pictures of a-CC tissues sections stained for C3d, Stat3 and GFP (a-f) and stained for C3d, S100a10 and GFP (g-l). (M) Graphic representation of C3d and Stat3 co-expressing cells in the a-CC. (n) Graphic representation of the number of C3d+/S100a10+/GFP+ and C3d+/S100a10- astrocytes in the a-CC indicating temporal dynamics and changes induced upon medrysone treatment (red bars: C3d+/Stat3-/GFP+; purple bars C3d+/Stat3+/GFP+; blue bars: C3d+/S100a10+/GFP+ cells; green bars: C3d+/S100a10-/GFP+ cells). White arrows point to cell nuclei. Bars correspond to mean cell numbers per mm² ± standard error of the mean (SEM). Statistical significance was calculated using a two-way ANOVA with multiple comparisons Bonferroni post-test (**p* < 0.05, ***p* < 0.01, and ****p* < 0.001). Number of animals *n*=5 (m, n). Exact *p*-values according to sequence from left to right: m: red bars: (*p*=0.0004107110343508). purple bars: (*p*=0.000056496386376, *p*=0.000003680985889, *p*=0.031174401322527). n: blue bars: (*p*=0.002451376341613, *p*=0.00060730463184, *p*=0.033987226291329, *p*=0.009878307898806). green bars: (*p*=0.000005242490508, *p*=0.0000000000000286, *p*<0.0000000000000001, *p*=0.00147922066168, *p*=0.0000000000243146, *p*=0.000000000000024, *p*=0.015520259581564, *p*=0.000070506774492).

Discussion

Medrysone is an FDA-approved corticosteroid, designated as a topical anti-inflammatory agent for ophthalmic use.⁵⁴⁻⁵⁵ Details on its activity in a neurological context are scarce and limited to a

positively regulated MBP expression in cultured Olig2 cells.⁵⁶ Nevertheless, medrysone was recently identified as an oligodendrogenesis promoting molecule in a pharmacogenomic study aiming at NSCs lineage manipulation.³³

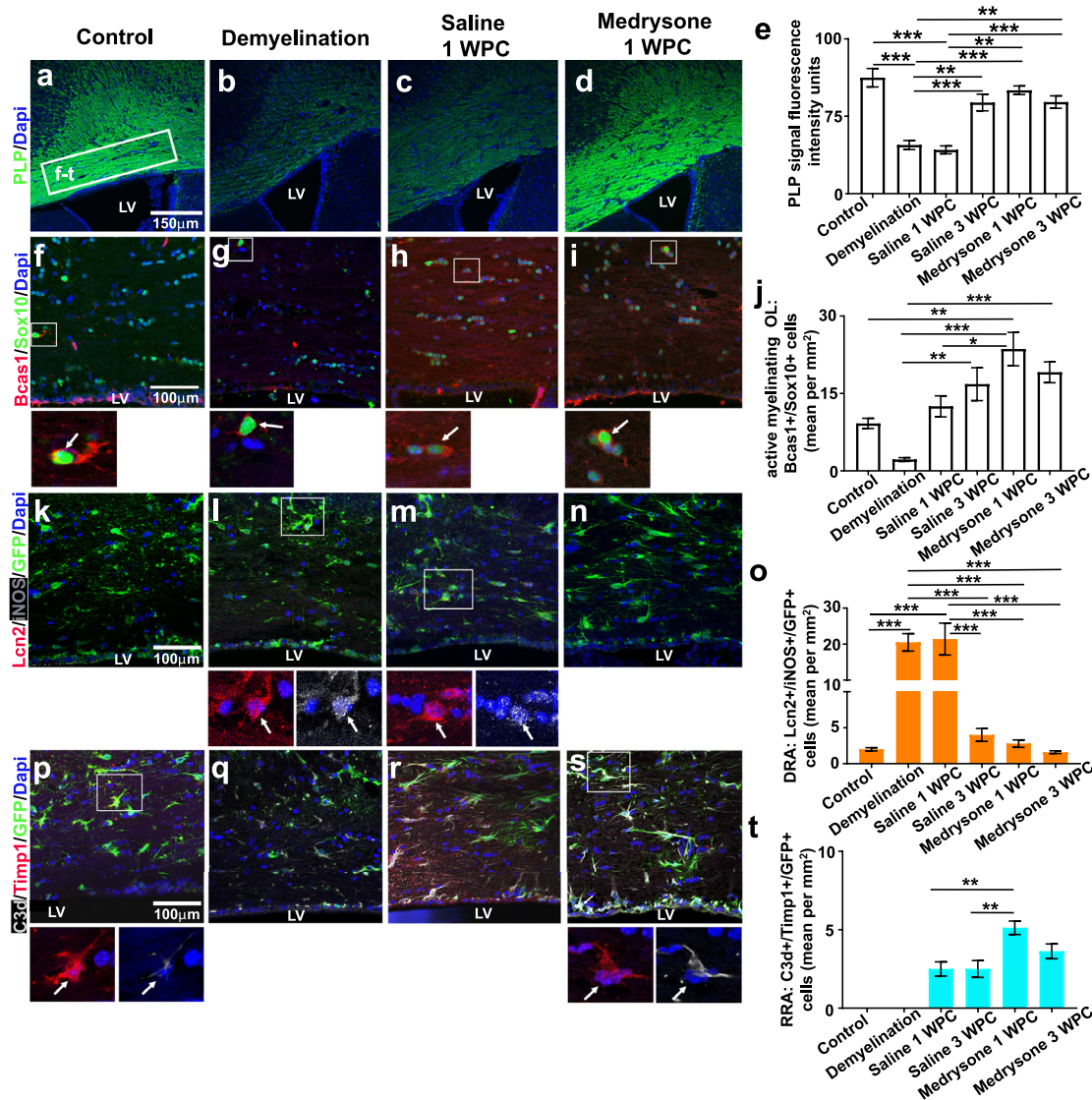


Figure 6. Medrysone treatment accompanies PLP recovery and remyelination-related astrogliosis at the corpus callosum adjacent to the dorsal SVZ. (a-d) Representative pictures showing PLP expression at the a-CC. (e) Quantification of PLP fluorescence intensity units revealed a demyelination induced decrease of PLP expression and a medrysone enhanced recovery of PLP levels. Representative photomicrographs of active myelinating OLs at the a-CC (Sox10+/Bcas1+). Quantification of active myelinating OLs at the a-CC (j) revealed a decrease of these cells during demyelination and medrysone to strongly counteract this effect. (k-n) Representative photomicrographs of DRAs (Lcn2+/iNOS+/GFP+) at the a-CC. (o) Quantification of DRA shows enhancement of this phenotype over demyelination and saline 1 WPC. (p-s) Representative photomicrographs of RRAs (C3d+/Timp1+/GFP+). (t) Quantification of RRA revealed that medrysone increased this phenotype at the early recovery phase. Abbreviations: Lateral ventricle (LV), demyelination related astrocytes (DRA), remyelination related astrocytes (RRA). Bars (e) correspond to PLP mean signal fluorescence intensity \pm standard error of the mean (SEM), bars in (g, o, t) correspond to mean cell numbers per $\text{mm}^2 \pm$ standard error of the mean (SEM). Statistical significance was calculated using a two-way ANOVA with multiple comparisons Bonferroni post-test ($*p < 0.05$, $**p < 0.01$, and $***p < 0.001$). Number of animals $n=5$ (e, j, o), $n=4$ (t). Exact p -values according to sequence from left to right: e: ($p=0.000006352482916$, $p=0.000002232001001$, $p=0.002400718707233$, $p=0.000115165255505$, $p=0.002114723859805$, $p=0.000711683124652$, $p=0.000036763007099$, $p=0.00062825077472$). j: ($p=0.003491161340599$, $p=0.003020739853541$, $p=0.000026903857775$, $p=0.000581789413022$, $p=0.03812643142709$). o: ($p=0.000012264417485$, $p=0.000006109495876$, $p=0.00006100471827$, $p=0.000023087347467$, $p=0.000008980415351$, $p=0.000029360883258$, $p=0.000011341827324$, $p=0.000004504968109$). t: ($p=0.006949092405986$, $p=0.006949092405986$).

We here describe that medrysone application *in vivo* promotes myelin repair activities in a chronic demyelination set-up leading to an accelerated and more efficient restoration of mature cell numbers, nodal structures and myelin content. Of note medrysone also restored body weight of treated animals (data not shown). Although in most cases such a regenerative activity is linked to direct effects on resident OPCs, our investigations using primary OPCs failed in demonstrating any promotion of oligodendroglial maturation at different levels (morphology, gene expression, myelin protein production; see Figure S1) which contradicts earlier findings using the Oli-neu cell line population.⁵⁶ Moreover, medrysone did not affect cultured primary OPC cell numbers or proliferation rates (data not shown). Apart from providing evidence that the medrysone-mediated remyelinating effects are most likely not directly attributed to resident oligodendroglia these observations also question the validity of functional screening approaches performed using immortalized cell lines. It rather supports the notion that for a translational output primary cells derived from different species are better suited⁵⁶ as recently shown by us.^{32,38}

We subsequently monitored astrocytes and SVZ-dependent astrogenic progeny at different sites within and adjacent to the corpus callosum and found a dynamic regulation of different cellular subpopulations to occur and to contribute to myelin repair. Our observations revealed that the numbers of GFP-positive cells (corresponding to either resident Gfap expressing astrocytes or stem cell derivatives) did not change over time in CCJ, while at a-CC and d-SVZ sites (see Figure 1c for anatomic guidance), cell numbers were more variable (Figure 3), thus suggesting a prominent contribution from the niche. This is additionally confirmed by medrysone rescuing and enhancing type B cell numbers (Egfr+/GFP+) at the d-SVZ of demyelinated mice (Figure S5). Moreover, we set-out to understand the heterogeneity across reactive astrocyte subpopulations within these tissues and their possible co-relation with de- or remyelination. Prior to the here presented *in vivo* approach, we also investigated medrysone's effects on rat cortex astrocyte polarization and activation. This clearly revealed that astrocytes can sense medrysone, that there is no reaction in terms of cell numbers but that this corticosteroid effectively decreases the number of neurotoxic astrocytes (Gfap+/C3d+) in response to TNF- α (Figure S2e, S2f) accompanied by decrease of A1/neurotoxic transcripts such as C3, and IL-6 (Figure S2h), thus indicating that also *in vivo* astrocytes are key to its mode of action.

Indeed, reactive astrogliosis and myelin damage occur simultaneously during acute demyelination^{57–60} and ablation of astrogliosis can be beneficial for remyelination⁵⁹ by either diminishing CPZ toxicity or via reduction of NF- κ B activation in astrocytes.⁶¹ However, over time reactive astrocytes were also found to be

crucial for myelin clearance and hence facilitating oligodendrocyte and myelin replacement^{43,62–65}; (Figures 4–6, S3). Of note, Lcn2 ablation in experimental autoimmune encephalomyelitis (EAE) animals was found to reduce demyelination, via diminishing metalloproteinases production.⁶⁶ We found that CPZ-diet also induced demyelination at the a-CC (Figure 6), which is recovered by medrysone earlier at 1 WPC. Over CPZ diet, demyelination related astrocytes (DRA; Lcn2+/iNOS+/GFP+) will exclusively populate the demyelinated a-CC (Figures 6g, 6j). Moreover, DRAs were strongly reduced upon medrysone treatment (Figure 6j). During the recovery phase, astrocytes were naturally losing such signatures or presented a hybrid phenotype simultaneously expressing neurotoxic and neuroprotective proteins (C3d, Stat3, S100a10 and Timpr, respectively).^{28,29} Medrysone application, on the one hand, reduced numbers of neurotoxic-like astrocytes (C3d+/S100a10-) while it simultaneously enhanced cell numbers with a neuroprotective character described below.

Astrocytic Stat3 signalling appears to be mandatory for reactivity in a myriad of neurodegenerative diseases,^{67,68} reducing inflammation and the spread of lesion during demyelination.^{29,68–70} C3d/Stat3 co-expressing astrocytes were found to be enhanced by medrysone at the dorsal horn SVZ (Figure S3), CCJ (Figure 4) and a-CC (Figure 5m) during the early recovery phase. S100a10 is a key A2 marker, identifying promyelinating astrocytes in MS lesions.⁶⁹ Nonetheless, neither in MS lesion astrocytes²⁶ nor in regenerated areas of the spinal cord⁷⁰ co-localization of C3d and S100a10 was reported, which is in contrast to the described presence of cells with a hybrid profile at CCJ, a-CC and middle d-SVZ in response to medrysone (Figure 5) indicating a strong and natural repair processes-exceeding effect of this corticosteroid. The recently published nuclear factor erythroid 2-related factor 2 (Nrf2) and transcription factor Mafg (Mafg), both being correlated to an anti- and pro-inflammatory signature in astrocytes, respectively,^{2,74,76} were also investigated. Two subtypes, Mafg/Nrf2+ and Mafg-/Nrf2- cells were found at the a-CC of control and saline 1 WPC groups, respectively (Figure S4). In the context of the anatomic domains investigated (see Figure 1c), these astrocyte subtypes were observed at the a-CC, only. Of note, this does not exclude the possibility that such astrocytes might also emerge from other brain areas.

An additional hybrid phenotype characterized by the presence of Timpr (RRA; C3d+/Timpr+/GFP+) was identified and found to be enhanced in response to medrysone particularly at the a-CC (Figure 6t). Timpr is naturally expressed by astrocytes,^{31,45} was recently shown to induce a myelinating profile in transplanted NSCs^{72,71}, is expressed by astrocytes in demyelinated white matter MS lesions and revealed to be down-regulated during CPZ-dependent demyelination.⁵³

Moreover, remyelination in acute and chronic demyelinated animals was shown to depend on astrocytic Timpr. ^{51,52} It is therefore conceivable that the here observed Timpr expressing reactive astrocytes, yet in a minor number and only localized at the a-CC, can contribute to myelin repair as evoked by medrysone (Figures 6s, 6t). Further investigations will be necessary to describe additional trophic entities related to here-presented astrocyte subpopulations that are also involved in the overall repair process. Future investigations upon the microglia-astrocyte axis following medrysone-treatment could illuminate if astrocyte heterogeneity occurs in co- or interdependency of microglia stimulation. ²⁵ This will also include investigations of medrysone acting directly on microglial cells as this has not been carried out so far. However, other corticosteroids have previously been shown to rescue an anti-inflammatory signature in these cells. ^{73–75} Likewise, a future investigation of medrysone on the EAE-clinical score [i.e., loss of tail tone, paralysis and cerebellar demyelination, which recapitulates MS disease features, ^{76,77} will be able to strengthen the inclusion of medrysone into upcoming clinical examinations.

Indeed, we here demonstrate that in a chronic demyelination set-up the application of the corticosteroid medrysone induces a robust myelin regeneration response marked by regulated astrocyte polarization and trophic factor expression. This study also suggests that this drug may be of use as a potential treatment for late-stage MS where regenerative processes increasingly fail. ^{1,32,77} Our study is currently limited to the fact that no interpretation of medrysone's anti-inflammatory effects on white matter repair could be considered. Additionally, it must be kept in mind that not all NSCs and astrocyte subtypes within the adult brain are fully covered by the GFAP-GFP driver. Finally, for a successful biomedical translation of these findings medrysone dependent responses of human brain cells need to be determined.

Contributors

Markley Silva Oliveira Junior performed the majority of all experiments, data analysis, data interpretation, text writing and figure design. Jessica Schira–Heinen has accessed and verified the data, in addition supported experimental design, data analysis, interpretation, text writing and figure design. Laura Reiche and Peter Göttele conducted primary OPC experiments and provided corresponding data analysis. Vanessa Cristina Meira de Amorim and Seulki Han provided support in data interpretation and data presentation. Isabel Lewen and Joel Gruchot executed primary astrocyte experiments and provided corresponding data analysis. Rainer Akkermann has accessed and verified the data and was involved in establishing the transgenic mouse strain and the cuprizone experiments. Kasum Azim was

involved in experimental design, funding acquisition, data analysis and interpretation. Patrick Küry (PK) conceived the final project and manuscript and took the final decision for submission. PK was involved in experimental design, funding acquisition, data analysis and interpretation and in text writing and figure composition. All authors read and approved the final version of the manuscript.

Data sharing statement

Any additional information required to reanalyse the data reported in this paper is available from the lead contact upon request.

Declaration of interests

The authors declare no competing interest.

Acknowledgements

We are grateful to Birgit Blumenkamp, Brigida Ziegler and Julia Jadasz for their excellent technical support.

Supplementary materials

Supplementary material associated with this article can be found in the online version at doi:[10.1016/j.ebiom.2022.104204](https://doi.org/10.1016/j.ebiom.2022.104204).

References

- 1 McGinley MP, Goldschmidt CH, Rae-Grant AD. Diagnosis and treatment of multiple sclerosis: a review. *JAMA - J Am Med Assoc.* 2021;325(8):765–779.
- 2 Wheeler MA, Clark IC, Tjon EC, et al. MAFG-driven astrocytes promote CNS inflammation. *Nature.* 2020;176(3):139–148.
- 3 Lo CH, Skarica M, Mansoor M, Bhandarkar S, Toro S, Pitt D. Astrocyte heterogeneity in multiple sclerosis: current understanding and technical challenges. *Front Cell Neurosci.* 2021;15:1–8.
- 4 Xing YL, Röth PT, Stratton JAS, et al. Adult neural precursor cells from the subventricular zone contribute significantly to oligodendrocyte regeneration and remyelination. *J Neurosci.* 2014;34(42):14128–14146.
- 5 Liu Q, Sanai N, Jin WN, La Cava A, Van Kaer L, Shi FD. Neural stem cells sustain natural killer cells that dictate recovery from brain inflammation. *Nat Neurosci.* 2016;19(2):243–252.
- 6 Hillis JM, Davies J, Mundim MV, Al-Dalahmah O, Szele FG. Cuprizone demyelination induces a unique inflammatory response in the subventricular zone. *J Neuroinflammation.* 2016;13(1):1–15.
- 7 Kriegstein A, Alvarez-Buylla A. The glial nature of embryonic and adult neural stem cells. *Vol. 32, Ann Rev Neurosci.* 2009;32:149–184.
- 8 Lim DA, Alvarez-Buylla A. The adult ventricular–subventricular zone (V-SVZ) and olfactory bulb (OB) neurogenesis. *Cold Spring Harb Perspect Biol.* 2016;8(5):1–33.
- 9 Menn B, Garcia-Verdugo JM, Yachine C, Gonzalez-Perez O, Rowitch D, Alvarez-Buylla A. Origin of oligodendrocytes in the subventricular zone of the adult brain. *J Neurosci.* 2006;26(30):7907–7918. 1.
- 10 Azim K, Fiorelli R, Zweifel S, et al. 3-dimensional examination of the adult mouse subventricular zone reveals lineage-specific microdomains. *PLoS One.* 2012;7(11).
- 11 Azim K, Akkermann R, Cantone M, Vera J, Jadasz JJ, Küry P. Transcriptional profiling of ligand expression in cell specific populations of the adult mouse forebrain that regulates neurogenesis. *Front Neurosci.* 2018;12:1–15.

- 12 Platel J-C, Gordon V, Heintz T, Bordey A. GFAP-GFP neural progenitors are antigenically homogeneous and anchored in their enclosed mosaic niche. *Glia*. 2008;57(1):66–78.
- 13 Benner EJ, Luciano D, Jo R, et al. Protective astrogenesis from the SVZ niche after injury is controlled by Notch modulator *Thbs4*. *Nature*. 2013;497(7449):369–373.
- 14 Faiz M, Sachewsky N, Gascón S, Bang KWA, Morshead CM, Nagy A. Adult neural stem cells from the subventricular zone give rise to reactive astrocytes in the cortex after stroke. *Cell Stem Cell*. 2015;17(5):624–634.
- 15 Butt AM, Rivera AD, Fulton D, Azim K. Targeting the subventricular zone to promote myelin repair in the aging brain. *Cells*. 2022;11(11):1809.
- 16 Brousse B, Magalon K, Durbec P, Cayre M. Region and dynamic specificities of adult neural stem cells and oligodendrocyte precursors in myelin regeneration in the mouse brain. *Biol Open. Company Biol*. 2015;4:980–992.
- 17 Cebrian-Silla A, Nascimento MA, Redmond SA, et al. Single-cell analysis of the ventricular-subventricular zone reveals signatures of dorsal and ventral adult neurogenic lineages. *Elife*. 2021;10:1–34.
- 18 Moraga A, Pradillo JM, García-Culebras A, et al. Aging increases microglial proliferation, delays cell migration, and decreases cortical neurogenesis after focal cerebral ischemia. *J Neuroinflammation*. 2015;12(1):11.
- 19 Baxi EG, Debruijn J, Jin J, et al. Lineage tracing reveals dynamic changes in oligodendrocyte precursor cells following cuprizone-induced demyelination. *Glia*. 2017;65(12):2087–2098.
- 20 Taraboletti A, Walker T, Avila R, et al. Cuprizone intoxication induces intrinsic alterations in oligodendrocyte metabolism independent of copper chelation. *Biochemistry*. 2017;56(10):1518–1528.
- 21 Pandur E, Pap R, Varga E, et al. Relationship of iron metabolism and short-term cuprizone treatment of *c57bl/6* mice. *Int J Mol Sci*. 2019;20(9).
- 22 Butti E, Bacigaluppi M, Chaabane L, et al. Neural stem cells of the subventricular zone contribute to neuroprotection of the corpus callosum after cuprizone-induced demyelination. *J Neurosci*. 2019;39(28):5481–5492.
- 23 Lohrborg M, Winkler A, Franz J, et al. Lack of astrocytes hinders parenchymal oligodendrocyte precursor cells from reaching a myelinating state in osmolyte-induced demyelination. *Acta Neuropathol Commun*. 2020;8(1):224.
- 24 Liddelow SA, Barres BA. Reactive astrocytes: production, function, and therapeutic potential. *Immunity*. 2017;46(6):957–967.
- 25 Liddelow SA, Guttenplan KA, Clarke LE, et al. Neurotoxic reactive astrocytes are induced by activated microglia. *Nature*. 2017;541(7638):481–487.
- 26 Tassoni A, Farkhondeh V, Itoh Y, Itoh N, Sofroniew MV, Voskuhl RR. The astrocyte transcriptome in EAE optic neuritis shows complement activation and reveals a sex difference in astrocyte *C3* expression. *Sci Rep*. 2019;9(1).
- 27 Harnis, Mairinger F, Fritsche L, Soub D, et al. Myelination in multiple sclerosis lesions is associated with regulation of bone morphogenetic protein 4 and its Antagonist Noggin. *Int J Mol Sci*. 2019;20(1):0–13.
- 28 Monteiro De Castro G, Deja NA, Ma D, Zhao C, Franklin RJM. Astrocyte activation via *stat3* signaling determines the balance of oligodendrocyte versus schwann cell remyelination. *Am J Pathology*. 2015;185(9):2431–2440.
- 29 Das S, Li Z, Noori A, Hyman BT, Serrano-Pozo A. Meta-analysis of mouse transcriptomic studies supports a context-dependent astrocyte reaction in acute CNS injury versus neurodegeneration. *J Neuroinflammation*. 2020;17(1):1–17.
- 30 Hasel P, Rose IVL, Sadick JS, Kim RD, Liddelow SA. Neuroinflammatory astrocyte subtypes in the mouse brain. Vol. 24. *Nature Neuroscience*. Springer Science and Business Media LLC; 2021:1475–1487.
- 31 Escartin C, Galea E, Lakatos A, et al. Reactive astrocyte nomenclature, definitions, and future directions. *Nat Neurosci Nat Res*. 2021;24(3):312–325.
- 32 Manousi A, Küry P. Small molecule screening as an approach to encounter inefficient myelin repair. *Curr Opin Pharmacol*. 2021;61:127–135.
- 33 Azim K, Angonin D, Marcy G, et al. Pharmacogenomic identification of small molecules for lineage specific manipulation of subventricular zone germinal activity. *PLoS Biol*. 2017;15(3):1–27.
- 34 Zhuo L, Sun B, Zhang CL, Fine A, Chiu SY, Messing A. Live astrocytes visualized by green fluorescent protein in transgenic mice. *Dev Biol*. 1997;187(1):36–42.
- 35 McCarthy KD, de Vellis J. Preparation of separate astroglial and oligodendroglial cell cultures from rat cerebral tissue. *J Cell Biol Rockefeller University Press*. 1980;85:890–902.
- 36 Kremer D, Heinen A, Jadasz J, et al. *P57Kip2* is dynamically regulated in experimental autoimmune encephalomyelitis and interferes with oligodendroglial maturation. *Proc Natl Acad Sci USA*. 2009;106(22):9087–9092.
- 37 Göttele P, Manousi A, Kremer D, Reiche L, Hartung HP, Küry P. Teriflunomide promotes oligodendroglial differentiation and myelination. *J Neuroinflammation*. 2018;15(1):1–12.
- 38 Manousi A, Göttele P, Reiche L, et al. Identification of novel myelin repair drugs by modulation of oligodendroglial differentiation competence. *EBioMedicine*. 2021;65:103276.
- 39 Schindelin J, Arganda-Carreras I, Frise E, et al. Fiji: An open-source platform for biological-image analysis. *Nat Methods*. 2012;9(7):676–682.
- 40 Faul F, Erdfelder E, Buchner A, Lang AG. Statistical power analyses using *G*Power* tests for correlation and regression analyses. *Behav Res Methods*. 2009;41(4):1149–1160.
- 41 Skripuletz T, Hackstette D, Bauer K, et al. Astrocytes regulate myelin clearance through recruitment of microglia during cuprizone-induced demyelination. *Brain*. 2013;136(1):147–167.
- 42 Schirmer L, Schafer PD, Bartels T, Rowitch D, Calabresi P. Diversity and function of glial cell types in multiple sclerosis. *Trends Immunol*. 2021;42(3):228–247.
- 43 Miyamoto N, Maki T, Shindo A, et al. Astrocytes promote oligodendrogenesis after white matter damage via brain-derived neurotrophic factor. *J Neurosci*. 2015;35(41):14002–14008.
- 44 Matias I, Morgado J, Gomes FCA. Astrocyte heterogeneity: impact to brain aging and disease. *Front Aging Neurosci*. 2019;11:1–18.
- 45 Clarke LE, Liddelow SA, Chakraborty C, Münch AE, Heiman M, Barres BA. Normal aging induces *A1*-like astrocyte reactivity. *Proc Natl Acad Sci U S A*. 2018;20(115(8)):E1896–E1905.
- 46 Allnoch L, Baumgärtner W, Hansmann F. Impact of astrocyte depletion upon inflammation and demyelination in a murine animal model of multiple sclerosis. *Int J Mol Sci*. 2019;20(16):3922.
- 47 Hou B, Zhang Y, Liang P, et al. Inhibition of the *NLRP3*-inflammatory prevents cognitive deficits in experimental autoimmune encephalomyelitis mice via the alteration of astrocyte phenotype. *Cell Death Dis*. 2020;11(5):1–16.
- 48 Lee S, Park JY, Lee WH, et al. *Lipocalin-2* is an autocrine mediator of reactive astrocytosis. *J Neurosci Soc Neurosci*. 2009;29:234–249.
- 49 Al Nimer F, Elliott C, Bergman J, et al. *Lipocalin-2* is increased in progressive multiple sclerosis and inhibits remyelination. *Neuroimmunol Neuroinflammation*. 2016;3(1):e191.
- 50 Zhao N, Xu X, Jiang, et al., et al. *Lipocalin-2* may produce damaging effect after cerebral ischemia by inducing astrocytes classical activation. *J Neuroinflammation*. 2019;16(1):1–15.
- 51 Ogier C, Creidy R, Boucraut J, Soloway PD, Khrestchatsky M, Rivera S. Astrocyte reactivity to Fas activation is attenuated in *TIMP-1* deficient mice. An *in vitro* study. *BMC Neurosci*. 2005;6:1–12.
- 52 Moore CS, Milner R, Nishiyama A, et al. Astrocytic tissue inhibitor of metalloproteinase-1 (*TIMP-1*) promotes oligodendrocyte differentiation and enhances CNS myelination. *J Neurosci*. 2011;31(16):6247–6254.
- 53 Houben E, Janssens K, Hermans D, et al. Oncostatin M-induced astrocytic tissue inhibitor of metalloproteinases-1 drives remyelination. *Proc Natl Acad Sci U S A*. 2020;117(9):5028–5038.
- 54 Spaeth GL. Hydroxymethylprogesterone: an anti-inflammatory steroid without apparent effect on intraocular pressure. *Arch Ophthalmol*. 1966;75(6):783–787.
- 55 Bedrossian RH, Eriksen SP. The treatment of ocular inflammation with medrysone. *Arch Ophthalmol*. 1969;81(2):184–191.
- 56 Porcu G, Serone E, De Nardis V, et al. *Clobetasol* and *halcinonide* act as smoothened agonists to promote myelin gene expression and *RxR γ* receptor activation. *PLoS One*. 2015;10(12):1–22.
- 57 Bribián A, Medina-Rodríguez EM, Josa-Prado F, et al. Functional heterogeneity of mouse and human brain OPCs: relevance for pre-clinical studies in multiple sclerosis. *J Clin Med*. 2020;9(6):1–21.
- 58 Steelman AJ, Thompson JP, Li J. Demyelination and remyelination in anatomically distinct regions of the corpus callosum following cuprizone intoxication. *Neurosci Res*. 2012;72(1):32–42.
- 59 Hibbits N, Yoshino J, Le TQ, Armstrong RC. Astroglialosis during acute and chronic cuprizone demyelination and implications for remyelination. *ASN Neuro*. 2012;4(6):393–408.

- 60 Orthmann-Murphy J, Call CL, Molina-Castro GC, et al. Remyelination alters the pattern of myelin in the cerebral cortex. *Elife*. 2020;9:1–61.
- 61 Madadi S, Pashbakhsh P, Tahmasebi F, et al. Astrocyte ablation induced by La-aminoadipate (L-AAA) potentiates remyelination in a cuprizone demyelinating mouse model. *Metab Brain Dis*. 2019;34:593–603.
- 62 Brück W, Pfortner R, Pham T, et al. Reduced astrocytic NF- κ B activation by laquinimod protects from cuprizone-induced demyelination. *Acta Neuropathol*. 2012;124(3):411–424.
- 63 Clemente D, Ortega MC, Melero-Jerez C, de Castro F. The effect of glia-glia interactions on oligodendrocyte precursor cell biology during development and in demyelinating diseases. *Front Cell Neurosci*. 2013;7(DEC):1–15.
- 64 Wheeler MA, Jaronen M, Covacu R, et al. Environmental control of astrocyte pathogenic activities in CNS Inflammation. *Cell*. 2019;176(3):581–596.e18.
- 65 Tognatta R, Karl MT, Fyffe-Maricich SL, et al. Astrocytes are required for oligodendrocyte survival and maintenance of myelin compaction and integrity. *Front Cell Neurosci*. 2020;14:74.
- 66 Nam Y, Kim JH, Seo M, et al. Lipocalin-2 protein deficiency ameliorates experimental autoimmune encephalomyelitis: The pathogenic role of lipocalin-2 in the central nervous system and peripheral lymphoid tissues. *J Biol Chem*. 2014;289(24):16773–16789.
- 67 Haim L Ben, Ceyzériat K, Sauvage MAC de, et al. The JAK/STAT3 pathway is a common inducer of astrocyte reactivity in Alzheimer's and Huntington's diseases. *J Neurosci*. 2015;35(6):2817–2829.
- 68 Herrmann JE, Imura T, Song B, et al. STAT3 is a critical regulator of astrogliosis and scar formation after spinal cord injury. *J Neurosci*. 2008;28(28):7231–7243.
- 69 Harnisch K, Teuber-Hanselmann S, Macha N, et al. Myelination in multiple sclerosis lesions is associated with regulation of bone morphogenetic protein 4 and its antagonist noggin. *Int J Mol Sci*. 2019;20(1):0–13.
- 70 Haindl MT, Köck U, Zeitelhofer-Adzemovic M, Fazekas F, Hochmeister S. The formation of a glial scar does not prohibit remyelination in an animal model of multiple sclerosis. *Glia*. 2019;67(3):467–481.
- 71 Samper-Agrelo I, Schira-Heinen J, Beyer F, et al. Secretome analysis of mesenchymal stem cell factors fostering oligodendroglial differentiation of neural stem cells in vivo. *Int J Mol Sci*. 2020;21(12):1–25.
- 72 Schira-Heinen J, Samper-Agrelo I, Estrada V, Küry P. Functional in vivo assessment of stem cell-secreted pro- oligodendroglial factors. *Neural Regen Res*. 2022;17(x):1–3.
- 73 Draheim T, Liessem A, Scheld M, Wilms F, Weissflog M, Denecke B, Clarner T. Activation of the astrocytic Nrf2/ARE system ameliorates the formation of demyelinating lesions in a multiple sclerosis animal model. *Glia*. 2016;64(12):2219–2230.
- 74 Harrison C. Steroids modulate microglia-mediated inflammation. *Nat Rev Drug Discov*. 2011;10(7):492–493.
- 75 Carrillo-De Sauvage MÁ, Maatouk L, et al. Potent and multiple regulatory actions of microglial glucocorticoid receptors during CNS inflammation. *Cell Death Differ*. 2013;20(11):1546–1557.
- 76 Cayre M, Falque M, Mercier O, Magalon K, Durbec P. Myelin repair: from animal models to humans. *Front Cell Neurosci*. 2021;15(04):1–20.
- 77 Greiner T, Kipp M. What guides peripheral immune cells into the central nervous system? *Cells*. 2021;10(8).